Preferential Eu Site Occupation and Its Consequences in the Ternary Luminescent Halides $AB_2I_5:Eu^{2+}$ (A = Li–Cs; B = Sr, Ba)

C. M. Fang and Koushik Biswas*

Department of Chemistry and Physics, Arkansas State University, State University, Arkansas 72467, USA

(Received 14 April 2015; revised manuscript received 14 May 2015; published 22 July 2015)

Several rare-earth-doped, heavy-metal halides have recently been identified as potential next-generation luminescent materials with high efficiency at low cost. $AB_2I_5:Eu^{2+}$ (A = Li–Cs; B = Sr, Ba) is one such family of halides. Its members, such as $CsBa_2I_5:Eu^{2+}$ and $KSr_2I_5:Eu^{2+}$, are currently being investigated as high-performance scintillators with improved sensitivity, light yield, and energy resolution less than 3% at 662 keV. Within the AB_2I_5 family, our first-principles-based calculations reveal two remarkably different trends in Eu site occupation. The substitutional Eu ions occupy both eightfold-coordinated $B1^{(VIII)}$ and the sevenfold-coordinated $B2^{(VII)}$ sites in the Sr-containing compounds. However, in the Ba-containing crystals, Eu ions strongly prefer the $B2^{(VII)}$ sites. This random versus preferential distribution of Eu affects their electronic properties. The calculations also suggest that in the Ba-containing compounds one can expect the formation of Eu-rich domains. These results provide atomistic insight into recent experimental observations about the concentration and temperature effects in Eu-doped $CsBa_2I_5$. We discuss the implications of our results with respect to luminescent properties and applications. We also hypothesize Sr, Ba-mixed quaternary iodides $ABa^{VIII}Sr^{VII}I_5:Eu$ as scintillators having enhanced homogeneity and electronic properties.

DOI: 10.1103/PhysRevApplied.4.014012

I. INTRODUCTION

Inorganic scintillators or phosphors doped with activators have important applications in the fields of radiation detection, fluorescent lamps, flat-panel displays, and white light-emitting diodes [1–3]. The key performance criteria of these materials are fundamentally related to the properties of the host crystal, the activator ion, and their collective role in carrier recombination and light emission. The emitted light should be fast, with limited self-absorption enabling the use of large crystals. It should also be efficiently integrated with the sensitivity spectrum of the photodetector (e.g., photomultiplier tube or photodiode) for ideal signal processing and readout. These specialized requirements along with cost considerations have given rise to experimental and theoretical efforts focused on developing new scintillators that satisfy the varying demands from diverse areas such as nuclear security, medical imaging, displays and lighting, petroleum explorations, high-energy physics, and geophysics.

Eu is a widely used luminescent center (activator) in oxide, nitride, and halide scintillators, emitting light at different wavelengths depending upon the type of application [1–4]. Recently, there has been additional progress in Eu-doped alkaline-earth-metal-containing materials, including binary and ternary halides, e.g., $CsBa_2I_5:Eu^{2+}$ and $KSr_2I_5:Eu^{2+}$, and $SrI_2:Eu^{2+}$ [5–16]. These halides have an improved light yield, favorable decay times, and an energy resolution less than 3% at 662 keV—making them prime candidates for a variety of applications. Therefore, the knowledge about Eu dopability and distribution and its effect on the energy-transfer mechanism is important to the design and optimization of new scintillators. Since the discovery of the scintillating properties of $CsBa_2I_5:Eu^{2+}$ (light yield reports in the range 80 000–102 000 photons/MeV and an energy resolution about 3.9%–2.3% at 662 keV) [9–11,13,14], ternary alkali-metal–alkaline-earth-metal iodides, e.g., $AB_2I_5:Eu^{2+}$ (A = alkali metal, B = Sr, Ba) have become a subject of interest [5,7–14]. Shirwadkar *et al.* prepare sizable $CsBa_2I_5:Eu^{2+}$ single crystals with different Eu^{2+} doping concentrations [11]. Alekhin *et al.* investigate temperature and concentration effects on the properties of $CsBa_2I_5:Eu^{2+}$ crystals [14]. $KSr_2I_5:Eu^{2+}$ was also recently found to exhibit advanced scintillation properties [5,7]. In particular, these crystals are also reported to be less hygroscopic compared to the well-known binary halides $LaBr_3:Ce^{3+}$ and $SrI_2:Eu^{2+}$ [9]. The possibility to grow large crack-free crystals—having no self-activity—at a relatively lower cost makes the $AB_2I_5:Eu^{2+}$ family a potential set of candidates for the next generation of scintillators.

Beck and co-workers investigated the AB_2I_5 family in the 1980s [17]. The observed AB_2I_5 crystals are isostructural with $TlPb_2Cl_5$ [9,17–19]. Bourret-Courchesne *et al.* determine the crystal structure of $CsBa_2I_5$ to be monoclinic with space group $P2_1/c$ [9]. In the crystal, there are two distinct crystallographic sites for alkaline-earth-metal B atoms (referred to here as the eightfold-coordinated $B1^{(VIII)}$ and sevenfold-coordinated $B2^{(VII)}$) and five different

*kbiswas@astate.edu

 © 2015 American Physical Society

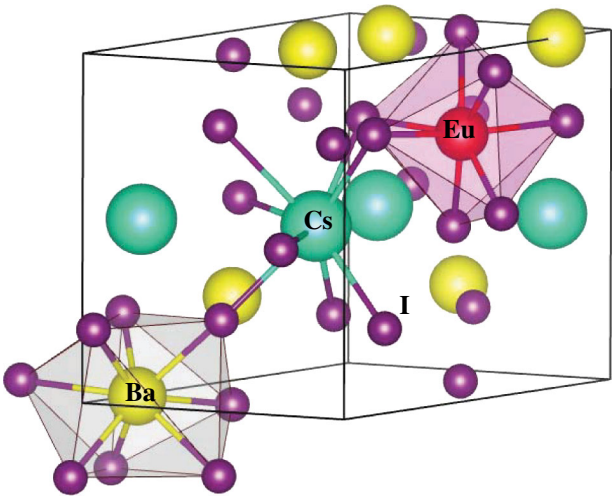

FIG. 1. Schematic crystal structure and coordination of metal atoms in $CsBa_2I_5:Eu^{2+}$. Here, Ba occupies a $B1^{(VIII)}$ site, and Eu is at a $B2^{(VII)}$ site.

Wyckoff sites for iodine. Figure 1 shows the coordination of the cations in $CsBa_2I_5:Eu^{2+}$, where the Ba occupies a $B1^{(VIII)}$ site and Eu is at a $B2^{(VII)}$ site. Although several recent experimental reports exist on the crystal growth and scintillation measurements [5,7,9–14], knowledge about the ternary $AB_2I_5:Eu^{2+}$ family is still limited. Parameter-free first-principles methods have been applied to the binary alkali-metal or alkaline-earth-metal halides and mixed alkali-metal halides [20–28]. To our knowledge, there are no further reports on theoretical simulations on the $AB_2I_5:Eu^{2+}$ crystals, especially on the Eu distribution and its consequences on electronic properties.

Here, we show that within the $AB_2I_5:Eu^{2+}$ (A = Li–Cs; B = Sr, Ba) compounds there is a striking difference in Eu distribution between the Sr- and Ba-containing crystals. The Eu ions energetically prefer the $B2^{(VII)}$ over the $B1^{(VIII)}$ sites in the Ba-containing compounds. No such preference is observed in the Sr-containing compounds. Furthermore, the possibility of Eu-rich domains in the Ba-containing crystals is revealed from our first-principles calculations. The obtained information is useful to understand the Eu-doping mechanism in these compounds. Finally, we discuss the possibility of Sr, Ba-mixed quaternary iodides of the type $ABa^{VIII}Sr^{VII}I_5:Eu$ having enhanced homogeneity and electronic properties for a better light yield and decay time.

II. COMPUTATIONAL DETAILS

All calculations are performed by using density-functional theory (DFT) within the projector-augmented-wave method [29,30] and the (spin-polarized) generalized gradient approximation (GGA) [31], as implemented in the Vienna *ab initio* simulation package (VASP) [32,33]. The standard approximations to density functionals, such as the local (spin-polarized) density-functional approximation and the GGA, often fail to describe systems with localized electrons, in this case Eu $4f$. The strongly localized Eu $4f$ orbitals are treated by using the Hubbard U approach by considering the on-site Coulomb interactions [34]. We use the rotationally invariant method [35] with an effective on-site interaction $U_{\text{eff}} = 2.5$ eV. The major effect of values of the parameter U_{eff} is to separate the occupied Eu^{2+} $4f^7$ orbitals (one spin orientation) from the unoccupied f levels (other spin orientation). Recently, Chaudhry and co-workers studied the localized Eu^{2+} $4f$ states in a series of alkali-metal and alkaline-earth-metal halides that match with experimental observations and concluded $U_{\text{eff}} = 2.2$–2.5 eV [36]. In the present work, we adopt an $U_{\text{eff}} = 2.5$ eV for better representation of the $5d$-$4f$ luminescence observed in these compounds. The spin-orbital-coupling effects are checked for the hosts and found to mainly affect the bandwidths of the valence bands, decreasing the energy gap by about 0.2–0.3 eV, but to be insignificant on total energies and magnetic properties.

In our calculations, we employ the pseudopotentials which include the semicore electrons as part of the valence states. Tests for other related potentials containing different semicore electrons are performed, and we find no significant differences. The cutoff energy of the wave functions is 237 eV. The electronic wave functions are sampled on a $3 \times 3 \times 2$ grid with eight irreducible k points in the Brillouin zone of the monoclinic AB_2I_5 crystals by using the Monkhorst and Pack method [37]. Tests of k-mesh density and cutoff energies show good convergence.

III. RESULTS AND DISCUSSION

A. Structural optimization

Experiments show that $CsBa_2I_5$ [9] and KSr_2I_5 [5,7], the two AB_2I_5 members investigated as bright scintillators, have a monoclinic crystal structure ($NH_4Pb_2Cl_5$ type) [17–19]. Therefore, we adopt the same structure for the rest of the AB_2I_5 family (Fig. 1). The experimental lattice parameters of $CsBa_2I_5$ are $a = 10.541$ Å, $b = 9.256$ Å, $c = 14.637$ Å, and $\beta = 90.194°$ [9]. These are slightly smaller than our PBE GGA optimized values ($a = 10.745$ Å, $b = 9.462$ Å, $c = 15.136$ Å, and $\beta = 89.79°$). This is not unusual, since GGA generally overestimates the lattice parameters of crystals [38,39].

The DFT calculations show that all the AB_2I_5 hosts are semiconductors with energy gaps being about 3.5–3.8 eV, which are underestimated by the GGA methods [29–33,38–40]. We also employ a hybrid functional (PBE0) [40], a "beyond DFT" technique to provide better electronic properties of the hosts. The PBE0 calculations produce an energy gap of 5.46 eV for $CsBa_2I_5$, which is significantly larger than the PBE GGA result (3.8 eV) and agrees closely with the experimentally estimated value of 5.2–5.5 eV [14]. The tops of the valence bands are dominated by I $5p$ states, while the conduction band edges

are dominated by Sr $4d$ or Ba $5d$ states with some mixing of Li $2s$, Na $3s$, K $4s$ or $3d$, Rb $4d$, Cs $5d$ characters for $A = \mathrm{Li}$ to Cs, respectively. In the Eu-doped compounds, the half-filled Eu $4f^7$ states take on a spin-aligned configuration with the occupied levels appearing inside the host band gap, and the empty f states remain inside the conduction band. The I p states at the valence band maximum have a small dispersion which favors hole localization. The d character of the Ba or Sr dopant site atoms near the conduction band minimum (CBM) is crucial to the Eu^{2+} $5d$-$4f$ emission (see Sec. III C, Fig. 4 for more details) [41].

B. Preferential Eu occupation in Ba-containing compounds

Upon Eu doping in the conventional cell of the AB_2I_5 hosts (approximately 3 at. % Eu), the activator ion may substitute a B^{2+} (Sr^{2+} or Ba^{2+}) ion at either of the available $B1^{(\mathrm{VIII})}$ or $B2^{(\mathrm{VII})}$ sites. Figure 2 shows the total energy differences $(E_{B2} - E_{B1})$ between Eu at $B2^{(\mathrm{VII})}$ (E_{B2}) and that of Eu at $B1^{(\mathrm{VIII})}$ (E_{B1}). Negative values signify that Eu at $B2^{(\mathrm{VII})}$ is energetically more stable. The behavior of the Ba-containing crystals is strikingly different from that of the Sr-containing crystals. The energy differences $(E_{B2} - E_{B1})$ for the Sr-containing crystals remain almost invariant as the alkali-metal ions change from Li (−14 meV) to Cs (−21 meV), with $B2^{(\mathrm{VII})}$ sites being marginally favored. Meanwhile, in the Ba-containing crystals, the magnitude of $(E_{B2} - E_{B1})$ shows an increasing trend from Li, Na, to K (−104, −147, and −198 meV, respectively) and then decreasing through Rb and Cs (−178 and −143 meV, respectively). To test for cell-size or concentration effects, we also calculate Eu substitution at $B1^{(\mathrm{VIII})}$ or $B2^{(\mathrm{VII})}$ sites inside a $2a_0 \times 2b_0 \times 1c_0$ $CsBa_2I_5$ supercell (21.42 × 18.86 × 15.08 Å [3]; a_0, b_0, and c_0 are the lattice parameters of a conventional cell) containing

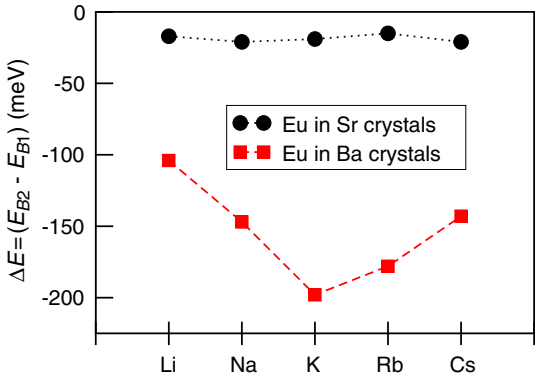

FIG. 2. Calculated energy differences $(E_{B2} - E_{B1})$ of Eu occupation at the $B2^{(\mathrm{VII})}$ sites with respect to that of the $B1^{(\mathrm{VIII})}$ sites in the different $AB_2I_5:Eu^{2+}$ compounds. A negative value of the energy means that Eu at $B2^{(\mathrm{VII})}$ is energetically favored.

128 atoms (approximately 0.8 at. % Eu). The calculations show that $(E_{B2} - E_{B1})$ is −146 meV, which is close to the value obtained in a conventional cell used here (−143 meV). These results indicate that, in ASr_2I_5 crystals, Eu occupies both $B1^{(\mathrm{VIII})}$ and $B2^{(\mathrm{VII})}$ sites, while, in Ba-containing compounds, Eu at $B2^{(\mathrm{VII})}$ is energetically preferred over the $B1^{(\mathrm{VIII})}$ site (see Fig. 1).

To understand the origin of the significantly different behavior among the Ba-containing and Sr-containing compounds, we analyze the local chemical bonds of the alkaline earth metals and the substitutional Eu dopants when they are coordinated at the $B1^{(\mathrm{VIII})}$ and $B2^{(\mathrm{VII})}$ sites. We use KBa_2I_5 and KSr_2I_5 as examples because of the largest energy difference between the two as seen in Fig. 2. Table I lists the calculated Ba—I, Sr—I, and Eu—I bond lengths in KBa_2I_5 and KSr_2I_5, when they occupy the available $B1^{(\mathrm{VIII})}$ or $B2^{(\mathrm{VII})}$ sites. The Eu—I distances in EuI_2 are also shown for comparison. There are two phases of EuI_2. One is orthorhombic, and the other is monoclinic [42,43]. In both forms, the Eu ions are sevenfold coordinated. In Table I, the Eu—I bond lengths in the orthorhombic cell are listed [42]. Calculated host energy gaps (E_g), the gap between the half-occupied Eu $4f$ and the conduction band minimum (hereinafter $4f$ CBM), and the orbital character of the CBM are also given in Table I. In KBa_2I_5, the $Ba1^{(\mathrm{VIII})}$—I interatomic distances range from 3.58 to 3.68 Å (average 3.62 Å), and $Ba2^{(\mathrm{VII})}$—I distances range from 3.42 to 3.70 Å (average 3.52 Å). $KBa_2I_5:Eu^{2+}$ has $Eu1^{(\mathrm{VIII})}$—I bond lengths ranging from 3.43 to 3.53 Å (average 3.50 Å), while $Eu2^{(\mathrm{VII})}$—I lengths between 3.28 and 3.54 Å (average 3.38 Å). That is, on average, the Eu—I bonds are about 0.13 Å shorter than the corresponding Ba—I bonds. Meanwhile, in KSr_2I_5, the averaged $Sr1^{(\mathrm{VIII})}$—I bond length is 3.48 Å, and $Sr2^{(\mathrm{VII})}$—I is 3.38 Å. In $KSr_2I_5:Eu^{2+}$, we obtain an average $Eu1^{(\mathrm{VIII})}$—I distance of 3.46 Å and $Eu2^{(\mathrm{VII})}$—I distance of 3.36 Å, respectively. These are close to the Sr—I bond lengths at the corresponding sites. As shown by Shannon [44], the ionic radius of (eightfold-coordinated) Eu^{2+} (1.25 Å) is almost identical to that of (eightfold-coordinated) Sr^{2+} (1.26 Å) but significantly smaller (13.6%) than that of Ba^{2+} (1.42 Å). It is also known that Sr and Eu are similar chemically and that in halides Sr and Eu compounds with the same composition tend to have extended ranges of solid solution. Therefore, one may not expect large lattice strain when Eu replaces Sr, but strong local relaxation should occur when Eu substitutes at a Ba site. We should also point out that the sevenfold-coordinated Eu in EuI_2 have average bond lengths that are close to that of $Eu2^{(\mathrm{VII})}$—I bonds in $KBa_2I_5:Eu^{2+}$ (Table I) [42]. We conclude that the large size mismatch between Eu and Ba at the eightfold-coordinated site and the ability to form shorter sevenfold-coordinated $Eu2^{(\mathrm{VII})}$—I bonds are the likely reason for the preferential occupation of the $B2^{(\mathrm{VII})}$ sites in $KBa_2I_5:Eu^{2+}$. This trend is also true for other AB_2I_5 members. Moreover, there is an increasing trend in ionic

TABLE I. Important $B1^{(VIII)}$—I and $B2^{(VII)}$—I distances d in the KB_2I_5 hosts (B = Ba, Sr) and the corresponding Eu—I distances in the doped crystals, obtained from the GGA ($+U$) approach. Calculated Eu—I bond lengths in EuI_2 and the average $d(B\text{—I})/d(\text{Eu—I})$ bond lengths (b) are included. The host energy gap E_g, the gap between the half-filled Eu $4f$ and the conduction band minimum ($4f$ CBM), and dominating eigencharacters for the electronic states near CBM are also listed.

Compound	$d(B1^{(VIII)}\text{—I})/$ $d(\text{Eu}1^{(VIII)}\text{—I})$ (Å)	$d(B2^{(VII)}\text{—I})/$ $d(\text{Eu}2^{(VII)}\text{—I})$ (Å)	Eg or $4f$ CBM gap (eV)	Eigencharacter at CBM
		$KBa_2I_5:Eu^{2+}$		
KBa_2I_5 host	3.58–3.68 $b = 3.62$	3.42–3.70 $b = 3.52$	3.76	Ba1 $5d$; K $4s$ or $3d$
Eu at $B1^{(VIII)}$	3.43–3.53 $b = 3.50$		2.52	Ba 1 or Ba 2 $5d$; Eu $5d$; K $4s$ or $3d$
Eu at $B2^{(VII)}$		3.28–3.54 $b = 3.38$	2.29	Ba1 $5d$; Eu $5d$; K $4s$ or $3d$
		$KSr_2I_5:Eu^{2+}$		
KSr_2I_5 host	3.42–3.60 $b = 3.48$	3.27–3.52 $b = 3.38$	3.66	Sr1 $5s$, $4d$; K $4s$ or $3d$
Eu at $B1^{(VIII)}$	3.42–3.58 $b = 3.46$		2.48	Sr1 or Sr2 $5s$, $4d$; Eu $5d$; K $4s$ or $3d$
Eu at $B2^{(VII)}$		3.25–3.50 $b = 3.36$	2.21	Sr1 $5s$, $4d$; Eu $5d$; K $4s$ or $3d$
		EuI_2 [42]		
		3.30–3.46 $b = 3.37$	2.06	Eu $5d$

radii of (eightfold-coordinated) alkali-metal ions from Li^+ to Cs^+ (0.92–1.74 Å) [44]. Compared with the radius of Ba^{2+} (1.42 Å), which is closer to that of K^+ (1.51 Å), the trend of energy differences of the Eu occupation in the Ba compounds is understandable due to the volume effects caused by the A^+ ions.

C. Eu-rich domains in Ba-containing compounds

In addition to preferential Eu site occupation, our calculations reveal a tendency to form Eu-rich domains in the Ba-containing compounds. Figure 3(a) shows the calculated formation energy (ΔE_f) of the quaternary $Cs(B_{1-x}Eu_x)_2I_5$ crystals relative to the ternaries CsB_2I_5 (B = Sr or Ba) and $CsEu_2I_5$ as a function of Eu concentration, where

$$\Delta E_f = E[\text{Cs}(\text{B}_{1-x}\text{Eu}_x)_2\text{I}_5] - [(1\text{-}x)E(\text{CsB}_2\text{I}_5) + xE(\text{CsEu}_2\text{I}_5)]. \quad (1)$$

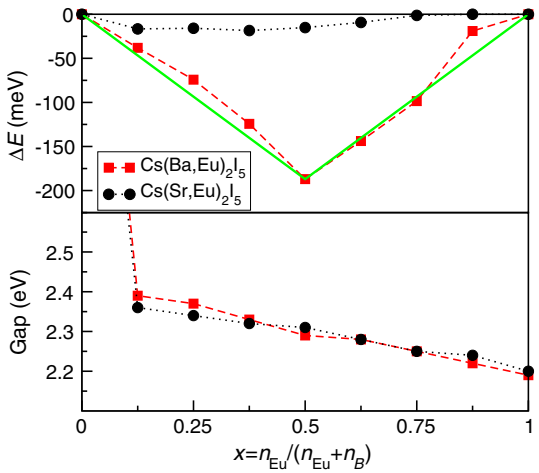

FIG. 3. Formation energy ΔE_f (top) and the $4f$ CBM energy gap (bottom) of $Cs(B_{1-x}Eu_x)_2I_5$ (B = Sr, Ba) as a function of Eu composition, $x = n_{Eu}/(n_{Eu} + n_B)$. n_{Eu} is the number of sites occupied by Eu, and n_B is the remaining number of sites for the B atom.

The Eu site occupation starts from the $B2^{(VII)}$ sites followed by the $B1^{(VIII)}$ sites. In the case of $Cs(Sr_{1-x}Eu_x)_2I_5$, where there is no energetic preference for Eu occupation, the formation energy varies within about 30 meV for the entire composition range. However, $Cs(Ba_{1-x}Eu_x)_2I_5$ shows a different trend: its stability increases while adjacent $B2^{(VII)}$ sites are being filled by Eu, forming nanometer-sized domains. The most stable configuration is at $x = 0.5$, when the Eu atoms completely occupy all available $B2^{(VII)}$ sites. By increasing the Eu concentration when no more of the favored $B2^{(VII)}$ sites are available, stability reduces. To further test the tendency to form Eu domains in $CsBa_2I_5$, we perform calculations for (a) a dilute case with 1-Eu in the $2a_0 \times 2b_0 \times 1c_0$ (128-atom) supercell and (b) 4-Eu occupying adjacent $B2^{(VII)}$ sites and aggregating within one of the four available conventional unit cell inside the 128-atom supercell. Our results confirm that the dispersed 1-Eu system is less stable than the system with the 4-Eu aggregate ($4 \times E_{1\text{-Eu}} - E_{4\text{-Eu-aggregate}} \approx 67$ meV). It can be surmised that Ba-containing crystals favor the formation of Eu domains occupying the adjacent $B2^{(VII)}$ sites.

Figure 3(b) shows the electronic consequence due to the formation of the Eu domains. In both compounds, there is a gradual narrowing of the $4f$ CBM energy gap when Eu occupies the adjacent $B2^{(VII)}$ sites followed by the $B1^{(VIII)}$ sites, decreasing by about 0.2 eV with increasing Eu

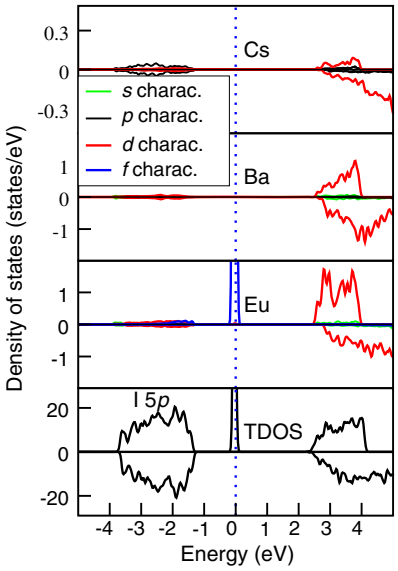

FIG. 4. Calculated total (TDOS) and partial density of states of the different atoms in $Cs(Ba_{0.5}Eu_{0.5})_2I_5$ around the Fermi level. The zero of energy is set at the top of the occupied Eu $4f^7$ states.

concentration. In order to elucidate the electronic picture resulting from the Eu domains, Fig. 4 shows the calculated total and partial (spin-polarized) density of states around the Fermi level of $Cs(Ba_{0.5}Eu_{0.5})_2I_5$ ($x = 0.5$ in Fig. 3). The Eu dopants completely occupy the available $B2^{(VII)}$ sites. The valence band has a width of 2.39 eV, being dominated by I $5p$ states, similar to those of the AB_2I_5 hosts. Meanwhile, Eu resembles a ground-state $4f^7$ electronic configuration creating a narrow band of spin-up electrons in the energy gap of the host, while the spin-down states remain inside the conduction band about 5 eV above the Fermi level (not shown). The bottom of the conduction band is mostly dominated by Eu $5d$ and Ba $5d$ states and some Cs $5d$ states mixing with I $5p$ orbitals. The Eu $5d$ states near the CBM are vital to the scintillation behavior. Most Eu-doped bright scintillators share this common hallmark where the bottom of the conduction band is an admixture of the d character from Sr or Ba alongside the substitutional dopant ion, enabling the $5d$-$4f$ emission [41]. The (spin-up) $4f$ CBM energy gap is about 2.3 eV. It is smaller than the corresponding $4f$ CBM gap of 2.4 eV in the more dilute case $Cs(Ba_{0.875}Eu_{0.125})_2I_5$, where Eu partially occupies the available $B2^{(VII)}$ site. The narrowing of the gap is a cumulative effect of the shift in the Eu $4f$ and $5d$ levels, which we emphasize will be more prominent in the Ba-containing compounds due to their proclivity towards Eu domains. Dorenbos observed an average Eu^{2+} Stokes shift of 0.27 ± 0.14 eV in Ba-containing compounds [4]. The smaller $4f$ CBM gap at the Eu domains may have important implications in the Stokes shift observed between the $4f$-$5d$ absorption and $5d$-$4f$ emission. The shift of the Eu $4f$ level while occupying the $B2^{(VII)}$ site is a testament to the incomplete screening by the outer s and p electrons from the crystal field of the host lattice.

The results shown in Fig. 3 support a model where the doped Ba-containing crystals prefer to form Eu-poor ($x \sim 0$) and Eu-rich regions ($x \sim 0.5$). The Eu-rich regions are the adjacent sevenfold-coordinated $Eu2^{(VII)}$—I domains. Note that the average $Eu2^{(VII)}$—I distances are shorter and closer to the Eu—I distances in EuI_2, compared to eightfold-coordinated $Eu1^{(VIII)}$—I bonds (see Table I). The shorter $Eu2^{(VII)}$—I distances and the increased overlap between the Eu $5d$ states accompanied by the incomplete shielding of the Eu $4f$ electrons causes gap narrowing between the half-filled Eu $4f^7$ and the CBM. The effect should be more pronounced in $CsBa_2I_5$ due the preferred $B2^{(VII)}$ sites and the formation of the Eu-rich domains compared to $CsSr_2I_5$ where no such aggregation is expected. This situation is depicted in Fig. 5(a), which shows a random Eu distribution (Sr-containing compounds). Figures 5(b) and 5(c) show Eu-poor and -rich regions, respectively, with accompanied gap narrowing at the Eu-rich domains (Ba-containing compounds). The presence of these domains in $CsBa_2I_5:Eu^{2+}$ and energy gap narrowing may explain the observed redshift of the Eu-emission peak [11,14]. We note that Fig. 3(b) shows similar band-gap narrowing in both Ba- and Sr-containing compounds, because the Eu occupation is deliberately started at the $B2^{(VII)}$ sites in both cases.

D. Consequences of Eu domains and possible Sr, Ba-mixed quaternary scintillators

Recent experimental reports on concentration and temperature effects of Eu in $CsBa_2I_5$ show some interesting trends. Varying the Eu concentration from 0.5% to 10.0% causes the luminescence peak to shift to longer

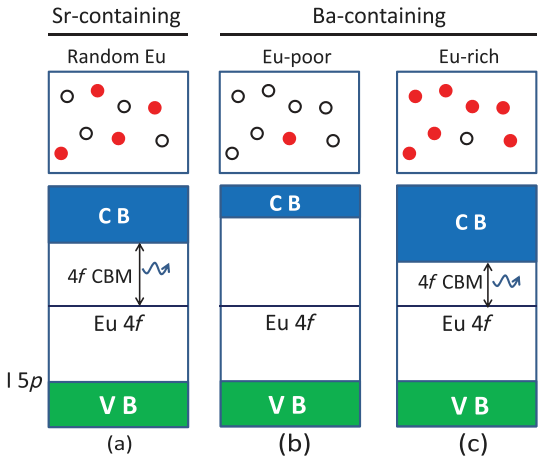

FIG. 5. Schematic of random Eu distribution (Sr-containing) and Eu-poor, Eu-rich domains (Ba-containing) in $AB_2I_5:Eu^{2+}$ compounds (B = Sr, Ba). Solid circles refer to Eu, and open circles are Sr or Ba. When B = Sr, random Eu distribution is expected as shown in (a). When B = Ba, Eu-poor and Eu-rich domains are expected (b),(c).

wavelengths under room-temperature conditions with increasing decay time (slower scintillation response) [11]. Another report observes that, at low Eu doping (0.5%), the emission peak in $CsBa_2I_5$ becomes broader but the peak position remains unchanged from 78 to 600 K. Increasing the temperature (600 K) and higher Eu concentration (5%) cause a redshift and broadening of the emission peak, accompanied by a longer decay time [14]. The redshift of the emission band and slower response are ascribed to Eu self-absorption. Indeed, this is a known problem where an overlap between the excitation and emission energies of Eu causes light trapping.

The (Eu-doped) $CsBa_2I_5$ crystals are grown from its melt, in the Bridgman method at around 600 °C, which is above its melting temperature [9–11,14]. At such temperatures, one expects homogeneous or random Eu distributions due to entropy. For low concentrations, Eu activators will distribute mainly at the $B2^{(VII)}$ sites in a random manner. The energy barriers and long distances between dopant ions will hinder the migration to form domains, and temperature does not play any significant role to produce Eu aggregation. When the Eu concentration increases (0.5%, 2%, 5%, and 10% in Ref. [11]), the statistical probability of Eu aggregation becomes higher. Figure 3 shows that $Cs(Ba^{VIII}Eu^{VII})_2I_5$ (12.5 at. % Eu) is stable relative to their parental ternaries. Eu ions in the Ba-containing compounds with concentration $0 < x < 12.5$ at. % are likely to form Eu-rich domains at temperatures below that of crystal growth. At these higher concentrations, especially at elevated temperature, the Eu ions are not frozen in to the lattice. They are able to overcome the diffusion barriers and redistribute, allowing the formation of Eu-rich ($x \sim 0.5$) and Eu-poor ($x \sim 0$) domains. As a consequence, the Eu-emission peak shifts to lower energy due to the $4f$ CBM gap narrowing [Figs. 5(b) and 5(c)]. This is observed by Alekhin *et al.* in $CsBa_2I_5$ with a high Eu concentration at an elevated temperature (5% Eu at 600 K) [14].

The single crystals are generally grown near the melting temperature and cooled down to room temperature [7–14]. As they are gradually cooled, the Eu ions form clusters or domains in $CsBa_2I_5:Eu$. This process will gradually change the local structure, as well as electronic and mechanical properties of the crystal. Clustering produces local lattice misfit, which may induce point defects, dislocations, and microcracks. That indicates damage on the electronic and mechanical properties of the crystals and further affects the reliability of devices.

Larger domains at medium or high Eu concentrations will also exacerbate self-absorption of Eu emission, which adds a slower component to the time response of the scintillator. A recent report shows that in $CsBa_2I_5:0.5\%$ Eu the photoluminescence decay time increases from 360 ns at 78 K to 910 ns at 600 K. At a higher concentration in $CsBa_2I_5:5\%$ Eu, it increases from 390 ns at 78 K to 3300 ns at 600 K [14]. Another report observes a similar concomitant increase in decay time with increasing Eu concentration [11], generally ascribing it to a smaller Stokes shift and larger overlap between the absorption and emission energies.

While the formation of the $Eu2^{(VII)}$ domains and the associated narrowing of the $4f$ CBM gap may help increase the Stokes shift of its $5d$-$4f$ emission, their aggregation, especially in larger Ba-containing crystals at higher Eu concentration, will aid self-absorption and deteriorate mechanical properties. This may ultimately compromise device performance. In order to have reliable scintillators, we require chemically homogeneous and large $ABa_2I_5:Eu^{2+}$ crystals with enhanced stability. The present calculations show the most stable crystal to be $Cs(Ba_{0.5}Eu_{0.5})_2I_5$, where all $B2^{(VII)}$ sites are occupied by Eu [Fig. 3(a)]. Based on their chemical similarity and our former discussions about ionic size and dopant site substitution between Sr^{2+} and Eu^{2+} in the crystals of the AB_2I_5 family, we propose Sr, Ba-mixed quaternary iodides, where Sr preferentially occupies the $B2^{(VII)}$ sites. That results in a $CsBa^{VIII}Sr^{VII}I_5$, or more generally $ABa^{VIII}Sr^{VII}I_5$. As a consequence, the mixed quaternary reveals an identical trend as seen in the case of $Cs(Ba,Eu)_2I_5$ [Fig. 3(a)]. Relative to the end members $CsBa_2I_5$ and $CsSr_2I_5$, replacing one Ba by Sr at the sevenfold-coordinated $B2^{(VII)}$ site results in a total energy gain of about 28 meV (or formation energy −28 meV). The energy gain continues with further Sr substitution until all the preferred $B2^{(VII)}$ sites are exhausted. Doping is also expected to be homogeneous with uniformly dispersed Eu replacing Sr at the $B2^{(VII)}$ sites in $ABa^{VIII}Sr^{VII}I_5:Eu$, eliminating the prospect of forming Eu-rich or -poor aggregates in the crystals. The Sr-Eu mixing should also serve to control Eu concentrations and further optimize its emission wavelength in the quaternary crystals.

One of the main tasks in nuclear security and nonproliferation is the proper identification of radioactive sources (threat versus nonthreat) and also its sensitivity to identify unknown gamma-emitting sources. The challenge is only compounded by the inherent complexity of the screening process (vehicles, people, and cargo) in a diverse setting. Therefore, an ability towards high spectroscopic resolution of gamma-ray energies and detection efficiency along with operational demands relating to size, weight, and ruggedness are some of the most important factors that need to be satisfied in this type of detectors. On the other hand, medical imaging applications such as those in computed tomography and positron emission tomography require enhanced spatial and time resolution [1,45]. Reliability and cost are common concerns in all applications. Currently, there seems to be a consensus on building commercially viable scintillators that have all the positive attributes of NaI:Tl detectors while possessing superior energy resolution, possibly approaching that of the more expensive and cryogenically cooled Ge detectors

(1% at 662 keV) [46]. Meeting this challenge will constitute a big technological advancement that will have immediate applications in radio-isotope identification devices. The initial reports on crystal growth, hygroscopicity, light yield, and energy resolution (less than 3% at 662 keV) thus far obtained from $CsBa_2I_5:Eu^{2+}$ and $KSr_2I_5:Eu^{2+}$ are comparable to the more distinguished binary counterparts $SrI_2:Eu^{2+}$ and $LaBr_3:Ce^{3+}$ and show enough promise to fulfil these demands [5,7,9–11,13,14]. However, inhomogeneous emission sites and nonradiative energy transfer between the inequivalent $B1^{(VIII)}$ and $B2^{(VII)}$ sites have been already noted as the drawbacks contributing to the complex decay profile and time response in $CsBa_2I_5:Eu^{2+}$ [10]. In this context, the proposed Sr, Ba-mixed $ABa^{VIII}Sr^{VII}I_5:Eu$ family is promising where the Eu^{2+} are likely to remain confined at the $B2^{(VII)}$ site, considering the fact that Eu in the ground state of EuI_2 is sevenfold coordinated [42,43]. While the scintillation decay times in the order of several hundred nanoseconds observed in $CsBa_2I_5:Eu^{2+}$ and $KSr_2I_5:Eu^{2+}$ are unsuitable for medical imaging techniques, the mixed cation approach mentioned here may help reduce self-absorption for faster response while resisting the formation of Eu-rich aggregates or domains. Other contributing factors such as better management of intrinsic and extrinsic defects from a materials standpoint and proper integration with a photosensor will also need to be addressed for optimum detector performance.

IV. CONCLUSIONS

Our first-principles DFT-based study on the Eu occupation in the AB_2I_5 (A = Li–Cs, B = Sr, Ba) host crystals demonstrates two distinct behaviors of activator distribution. In the Sr-containing crystals, Eu activators occupy both the $B1^{(VIII)}$ and $B2^{(VII)}$ sites. However, in the Ba-containing crystals, Eu favors the $B2^{(VII)}$ sites and shows a tendency towards forming Eu-rich domains. These domains may create crystal inhomogeneity and are also associated with $4f$ CBM energy gap narrowing, possibly causing the observed luminescence peaks shift to longer wavelengths while adding a slower component to the scintillation time response. Inhomogeneous distribution of the domains may be circumvented by employing a Sr, Ba-mixed quaternary iodide $ABa^{VIII}Sr^{VII}I_5:Eu$, where Sr and Eu both preferentially occupy the $B2^{(VII)}$ sites. This should allow better crystal quality and control over Eu content to improve the performance and proportional response of these scintillators.

ACKNOWLEDGMENTS

This material is based upon work supported by the U.S. Department of Homeland Security under Grant No. 2014-DN-077-ARI075-02. This research uses computational resources of the National Energy Research Scientific Computing Center and Arkansas State University. Computational resources at AState are partially funded from DNDO-NSF Grant No. ECCS-1348341. C. M. F. acknowledges support from National Security Technologies, LLC, under Contract No. DE-AC52-06NA25946 with the U.S. Department of Energy, and the Site-Directed Research and Development Program.

[1] C. Feldmann, T. Jüstel, C. R. Ronda, and P. J. Schimdt, Inorganic luminescent materials: 100 years of research and application, Adv. Funct. Mater. **13**, 511 (2003).

[2] P. A. Rodnyi, *Physical Processes in Inorganic Scintillators* (CRC Press, Boca Raton, FL, 1997).

[3] R. Chen and D. J. Lockwood, Developments in luminescence and display materials over the last 100 years as reflected in electrochemical society publications, J. Electrochem. Soc. **149**, S69 (2002).

[4] P. Dorenbos, Energy of the first $4f^7$-$4f^6$ 5d transition of Eu^{2+} in inorganic compounds, J. Lumin. **104**, 239 (2003).

[5] L. Stand, M. Zhuravleva, A. Lindsey, and C. L. Melcher, Growth and characterization of potassium strontium iodide: A new high light yield scintillator with 2.4% energy resolution, Nucl. Instrum. Methods Phys. Res., Sect. A **780**, 40 (2015).

[6] B. D. Milbrath, A. J. Peurrung, M. Bliss, and W. J. Weber, Radiation detector materials: An overview, J. Mater. Res. **23**, 2561 (2008).

[7] M. Zhuravleva, C. L. Melcher, L. Stand, A. Lindsey, H. Wei, C. Hobbs, and M. Koschan, High energy resolution scintillators for nuclear nonproliferation applications, Proc. SPIE Int. Soc. Opt. Eng. **V9213**, 921303 (2014).

[8] G. Gundiah, G. Bizarri, S. M. Hanrahan, M. J. Weber, E. D. Bourret-Courchesne, and S. E. Derenzo, Structure and scintillation of Eu^{2+}-activated solid solutions in the $BaBr_2 - BaI_2$ system, Nucl. Instrum. Methods Phys. Res., Sect. A **652**, 234 (2011).

[9] E. D. Bourret-Courchesne, G. Bizarri, R. Borade, Z. Yan, S. M. Hanrahan, G. Gundiah, A. Chaudhry, A. Canning, and S. E. Derenzo, Eu^{2+}-doped Ba_2CsI_5, a new high-performance scintillator, Nucl. Instrum. Methods Phys. Res., Sect. A **612**, 138 (2009).

[10] G. Bizarri, E. D. Bourret-Courchesne, Z. W. Yan, and S. E. Derenzo, Scintillation and optical properties of $BaBrI:Eu^{2+}$ and $CsBa_2I_5:Eu^{2+}$, IEEE Trans. Nucl. Sci. **58**, 3403 (2011).

[11] U. Shirwadkar, R. Hawrami, J. Glodo, E. V. D. van Loef, and K. S. Shah, Promising alkaline earth halide scintillators for gamma-ray spectroscopy, IEEE Trans. Nucl. Sci. **60**, 1011 (2013).

[12] M. S. Alekhin, D. A. Biner, K. W. Krämer, and P. Dorenbos, Optical and scintillation properties of $SrI_2:Yb^{2+}$, Opt. Mater. **37**, 382 (2014).

[13] M. Gascón, E. C. Samulon, G. Gundiah, Z. Yan, I. V. Khodyuk, S. E. Derenzo, G. A. Bizarri, and E. D. Bourret-Courchesne, Scintillation properties of $CsBa_2I_5$ activated with monovalent ions Tl+, Na+ and In+, J. Lumin. **156**, 63 (2014).

[14] M. S. Alekhin, D. A. Biner, K. W. Krämer, and P. Dorenbos, Optical and scintillation properties of $CsBa_2I_5:Eu^{2+}$, J. Lumin. **145**, 723 (2014).
[15] E. V. D. van Loef, P. Dorenbos, C. W. E. van Eijk, K. Kramer, and H. U. Gudel, High-energy-resolution scintillator: Ce^{3+} activated $LaBr_3$, Appl. Phys. Lett. **79**, 1573 (2001).
[16] N. J. Cherepy, G. Hull, A. D. Drobshoff, S. A. Payne, E. van Loef, C. M. Wilson, K. S. Shah, U. N. Roy, A. Burger, L. A. Boatner, W. S. Choong, and W. Moses, SrI_2 scintillator for γ-ray spectroscopy, Appl. Phys. Lett. **92**, 083508 (2008).
[17] H. P. Beck, G. Clicqué, and H. Nau, A study on AB_2X_5 compounds (A: K, In, Tl; B: Sr, Sn, Pb; X: Cl, Br, I), Z. Anorg. Allg. Chem. **536**, 35 (1986).
[18] G. Schilling and G. Meyer, Ternare Bromide und Iodide zweiwertiger Lanthanide und ihre Erdalkali-Analoga vom Typ AMX_3 und AM_2X_5, Z. Anorg. Allg. Chem. **622**, 759 (1996).
[19] I. Campostrini, F. Demartin, C. M. Gramaccioli, and P. Orlandi, Hephaistosite, $TlPb_2Cl_5$, a new thallium mineral species from La Fossa Crater, Vulcano, Aeolian Islands, Italy, Can. Mineral. **46**, 701 (2008).
[20] D. Åberg, B. Sadigh, and P. Erhart, Electronic structure of $LaBr_3$ from quasiparticle self-consistent GW calculations, Phys. Rev. B **85**, 125134 (2012).
[21] P. Erhart, A. Schleife, B. Sadigh, and D. Åberg, Quasiparticle spectra, absorption spectra, and excitonic properties of NaI and SrI_2 from many-body perturbation theory, Phys. Rev. B **89**, 075132 (2014).
[22] Q. Li, R. T. Williams, A. Burger, R. Adhikari, and K. Biswas, Search for improved-performance scintillator candidates among the electronic structures of mixed halides, Proc. SPIE Int. Soc. Opt. Eng. **9213**, 92130M (2014).
[23] D. J. Singh, Near optical isotropy in noncubic SrI_2: Density functional calculations, Appl. Phys. Lett. **92**, 201908 (2008).
[24] D. J. Singh, Structure and optical properties of high light output halide scintillators, Phys. Rev. B **82**, 155145 (2010).
[25] M. P. Prange, R. M. Van Ginhoven, N. Govind, and F. Gao, Formation, stability, and mobility of self-trapped excitations in NaI and $NaI_{1-x}Tl_x$ from first principles, Phys. Rev. B **87**, 115101 (2013).
[26] J. Bang, Z. Wang, F. Gao, S. Meng, and S. B. Zhang, Suppression of nonradiative recombination in ionic insulators by defects: Role of fast electron trapping in Tl-doped CsI, Phys. Rev. B **87**, 205206 (2013).
[27] M. H. Du, Chemical trends of electronic, and optical properties of ns^2 ions in halides, J. Mater. Chem. C **2**, 4784 (2014).
[28] R. Adhikari, Q. Li, R. T. Williams, A. Burger, and K. Biswas, DX-like centers in NaI:Tl upon aliovalent codoping, J. Appl. Phys. **116**, 223703 (2014).
[29] P. E. Blöchl, Projector augmented-wave method, Phys. Rev. B **50**, 17953 (1994).
[30] G. Kresse and J. Joubert, From ultrasoft pseudopotentials to the projector augmented-wave method, Phys. Rev. B **59**, 1758 (1999).
[31] J. P. Perdew, K. Burke, and M. Ernzerhof, Generalized gradient approximation made simple, Phys. Rev. Lett. **77**, 3865 (1996).
[32] G. Kresse and J. Hafner, Ab initio molecular-dynamics simulation of the liquid-metal–amorphous-semiconductor transition in germanium, Phys. Rev. B **49**, 14251 (1994).
[33] G. Kresse and J. Furthmller, Efficiency of ab-initio total energy calculations for metals and semiconductors using a plane-wave basis set, Comput. Mater. Sci. **6**, 15 (1996).
[34] J. Hubbard, Electron correlations in narrow energy bands, Proc. R. Soc. A **276**, 238 (1963).
[35] S. L. Dudarev, G. A. Botton, S. Y. Savrasov, C. J. Humphreys, and A. P. Sutton, Electron-energy-loss spectra and the structural stability of nickel oxide: An LSDA + U study, Phys. Rev. B **57**, 1505 (1998).
[36] A. Chaudhry, R. Boutchko, S. Chourou, G. Zhang, N. Grønbech-Jensen, and A. Canning, First-principles study of luminescence in Eu^{2+}-doped inorganic scintillators, Phys. Rev. B **89**, 155105 (2014).
[37] H. J. Monkhorst and J. D. Pack, Special points for Brillouin-zone integrations, Phys. Rev. B **13**, 5188 (1976).
[38] R. G. Parr and W. T. Yang, Density-functional theory of the electronic structure of molecules, Annu. Rev. Phys. Chem. **46**, 701 (1995).
[39] A. J. Cohen, P. Mori-Sánchez, and W. T. Yang, Challenges for density functional theory, Chem. Rev. **112**, 289 (2012).
[40] J. Heyd, G. S. Scuseria, and M. Ernzerhof, Hybrid functionals based on a screened Coulomb potential, J. Chem. Phys. **118**, 8207 (2003).
[41] P. Dorenbos, Thermal quenching of Eu^{2+} 5d–4f luminescence in inorganic compounds, J. Phys. Condens. Matter **17**, 8103 (2005).
[42] M. Krings, M. Wessel, and R. Dronskowski, EuI_2, a low-temperature europium(II) iodide phase, Acta Crystallogr. Sect. C **65**, i66 (2009).
[43] H. Baernighausen, H. Beck, H. W. Grueninger, E. T. Rietschel, and N. Schultz, Neue (AB_2)-strukturtypen mit siebenfach koordiniertem kation, Z. Kristallogr. **128**, 430 (1969).
[44] R. D. Shannon, Revised effective ionic radii and systematic studies of interatomic distances in halides and chalcogenides, Acta Crystallogr. Sect. A **32**, 751 (1976).
[45] Y. Wu, F. Meng, Q. Li, M. Koschan, and C. L. Melcher, Role of Ce^{4+} in the scintillation mechanism of codoped $Gd_3Ga_3Al_2O_{12}:Ce$, Phys. Rev. Applied **2**, 044009 (2014).
[46] K. E. Nelson, T. B. Gosnell, and D. A. Knapp, Report No. LLNL-TR-411374 2009.

View publication stats